An Investigation of Real-Gas and Multiphase Effects on Multicomponent Diesel Sprays

Federico Perini, Wisconsin Engine Research Consultants LLC
Stephen Busch, Sandia National Laboratories
Rolf D. Reitz, Wisconsin Engine Research Consultants LLC

Abstract

Lagrangian spray modeling represents a critical boundary condition for multidimensional simulations of in-cylinder flow structure, mixture formation and combustion in internal combustion engines. Segregated models for injection, breakup, collision and vaporization are usually employed to pass appropriate momentum, mass, and energy source terms to the gas-phase solver. Careful calibration of each sub-model generally produces appropriate results. Yet, the predictiveness of this modeling approach has been questioned by recent experimental observations, which showed that at trans- and super-critical conditions relevant to diesel injection, classical atomization and vaporization behavior is replaced by a mixing-controlled phase transition process of a dense fluid. In this work, we assessed the shortcomings of classical spray modeling with respect to real-gas and phase-change behavior, employing a multicomponent phase equilibrium solver and liquid-jet theory. A Peng-Robinson Equation of State (PR-EoS) model was implemented, and EoS-neutral thermodynamics derivatives were introduced in the FRESCO CFD platform turbulent NS solver. A phase equilibrium solver based on Gibbs free energy minimization was implemented to test phase stability and to compute phase equilibrium. Zero-dimensional flash calculations were employed to validate the solver with single- and multi-component fuels, at conditions relevant to diesel injection. The validation showed that 2-phase mixture temperature in the jet core can deviate up to 40K from the single-phase solution. Surface equilibrium with Raoult's law employed for drop vaporization calculation was observed to deviate up to 100% from the actual multiphase real-gas behavior. Liquid-jet spray structure in high pressure fuel injection CFD calculations was modeled using an equilibrium-phase (EP) Lagrangian injection model, where liquid fuel mass is released to the Eulerian liquid phase, assuming phase-equilibrium in every cell. Comparison to state-of-the-art modeling featuring KH-RT breakup and multicomponent fuel vaporization highlighted the superior predictive capabilities of the EP model in capturing liquid spray structure at several conditions with limited calibration efforts.

Introduction

In recent years, the classical theory of split-phase spray atomization for supercritical injections relevant to diesel engines has been subject to scrutiny by the spray research community [1]. Using high-fidelity experimental imagery, diesel sprays were found to deviate from conventional liquid column atomization with droplets towards a miscible-mixing regime where the two-phase liquid-vapor interface thickness is increased, surface tension forces are significantly reduced, and a diffusion-dominated mixing layer is formed, where local phase conditions are close to equilibrium.

Recent experimental evidence supports the need to extend diesel fuel injection modeling approaches to these regimes. For instance, Crua et al. [2] imaged the time evolution of drops detached from diesel fuel injection, and identified three mixing regions: via classical vaporization of nearly-spherical drops; via transitional mixing of strongly distorted drops; or via diffusive mixing with fading liquid-vapor interfaces. Neal and Rothamer [3] found that mixing-dominated behavior of diesel injections is found at several ambient conditions, fuels, and rates of injection, after the liquid core is disintegrated approximately at the breakup length. Manin et al. [4] imaged spray formation using the Engine Combustion Network Spray A injector at increasing pressures and temperatures, and found that no droplet and ligament formation could be seen at engine-like conditions, suggesting for the role of diminished surface tension to dominate this phenomenon. Dahms and Oefelein [5] developed a theory to explain the dominant parameters on these observed mixing regimes, and showed that the transition to mixing-dominated regimes has a similar temperature-pressure pattern for most fuels, occurring at most high-pressure conditions relevant to combustion devices, even though with a trend of increasing pressure for increasing fuel carbon number.

Based on these findings, modeling efforts have been attempted at capturing those effects with high-fidelity computational fluid dynamics (CFD) simulations: for example, Matheis and Hickel [6] developed a phase equilibrium solver and applied it to model Spray A injection using Large Eddy Simulation; Rodriguez et al. [7] coupled a molecular-based equation of state with a Riemann solver to simulate fuel injection in a two-dimensional domain. Others employ an engineering-level resolution approach focused on achieving accurate internal combustion engines simulations. This approach was pioneered by Trujillo et al. [8, 9], and later by Qiu and Reitz [10, 11] and Yue and Reitz [12]. In this paper, we developed on these engine-focused efforts to investigate real-gas and multiphase effects on multicomponent diesel fuel sprays.

The paper develops as follows. First, an explanation of the tools is given – an implementation of the Peng-Robinson Equation of State (EoS) and of the multi-phase equilibrium solver. This is followed by an assessment of the effects of computed multiphase equilibria for diesel primary reference fuel sprays on predicted gas- and vapor-phase fluid properties, and a discussion of the shortcomings of not including them in conventional spray modeling approaches. Then, a discussion of the application of phase equilibrium to engineering-size CFD simulation through the equilibrium-phase/liquid-jet Lagrangian model is shown.

10/16/2019

Simulation methodology

The FRESCO CFD solver [13] was employed as a framework for performing real-gas and multiphase simulations. The simulation platform is a modern Fortran toolkit which implements a parallel volume-of-fluid solver for the turbulent Navier-Stokes equations with automatic domain decomposition in body-fitted, topology-changing meshes. The solver implements state-of-the-art turbulence [14], spray [15] and chemistry models [16] and has been extensively validated for diesel spray and combustion simulations (see refs. [17, 18, 19]). In the current work, the solver was extended by including equation-of-state (EoS) neutral gas-phase thermodynamic derivatives and a multiphase Eulerian flow treatment with the single-fluid approach.

Equation of State

The Peng-Robinson Equation of State model [20] was employed for modeling non-ideal mixtures. This simple cubic equation of state characterizes non-ideal behavior of each species by adding two temperature-dependent parameters *a, b* to the ideal-gas equation:

$$p = \frac{RT}{\bar{v}-b} - \frac{a}{\bar{v}(\bar{v}+b)+b(\bar{v}-b)}, \qquad (1)$$

where $\bar{v}\ [cm^3/mol]$ is the molar volume, *R* the universal gas constant, and the species parameters

$$a = a(T) = \alpha \cdot 0.457235 \frac{R^2 T_c^2}{p_c}, \qquad (2)$$

$$b = 0.077796 \cdot R \frac{T_c}{p_c},$$

$$\alpha = \alpha(T) = \left[1 + \kappa\left(1 - \sqrt{\frac{T}{T_c}}\right)\right]^2,$$

$$\kappa = 0.37464 + \omega(1.54226 - 0.26992\omega),$$

each one being described by three constants: T_c and p_c are temperature and pressure at the critical point, and $\omega\ [-]$ is the molecular acentric factor. For a mixture of several components, the conventional van der Waals mixing rule was employed to obtain mixture-averaged coefficients [21]:

$$a = \sum_i^{n_s} \sum_j^{n_s} X_i X_j a_{ij},$$

$$a_{ij} = (1 - k_{ij})\sqrt{a_i}\sqrt{a_j}, \qquad (3)$$

$$b = \sum_i^{n_s} X_i b_i,$$

where X_i represent species mole fractions and k_{ij} optional binary interaction coefficients between species *i* and *j* in the mixture, set to zero by default. Note that the Peng-Robinson equation of state naturally generalizes to mixtures that contain ideal-gas species, such as commonly happens when employing large diesel combustion chemistry mechanisms. Here, real-gas information for several species may not be available, and for them, simply $a_i=b_i=0$. Since the number of ideal-gas species can be large, the set of real-gas species is pre-processed and flagged as 'active' in the EoS class, in order to save CPU time by avoiding unnecessary calculations. Table 1 reports select real-gas properties of species employed in the

current work. Whenever available, user-based coefficients are employed; otherwise, the FRESCO fuel library, which contains real-gas properties for core gas-phase air components plus tens of hydrocarbon species, is queried.

species	w [g/mol]	Tc [K]	Pc [bar]	ω [–]
hmn	226.45	692.0	15.3	0.55
nC$_{16}$H$_{34}$	226.45	720.6	13.2	0.78
N$_2$	28.01	126.2	34.0	0.04
CO$_2$	44.01	304.2	73.8	0.23
H$_2$O	18.02	647.3	220.0	0.31
O$_2$	31.998	154.6	50.4	0.02

Table 1. Summary of real-gas properties for species relevant to the current paper.

Compressibility. Mixture compressibility $z = p\bar{v}/(RT)$ is obtained by solving for the cubic EoS (see [8], eq. 36), using an analytical cubic equation solution. When multiple real roots are present and a specific phase type is requested, the phase identification criterion by Michelsen and Mollerup [22] is employed; otherwise, the Gibbs-minimizing phase type is considered. Figure 1 reports predicted Gibbs-minimizing compressibility of a DPRF58 (58% iso-cetane – hmn, 42% n-hexadecane) Diesel Primary Reference surrogate representing a CN=50.7 diesel fuel. This fuel has pseudo-critical properties: $T_c = 703.9K; p_c = 14.4\ bar$. The Peng-Robinson EoS is known to provide only approximate predictions of the near- and sub-critical ranges; for example, critical point compressibility of any species and mixtures is fixed. However, it was still employed because of its excellent phase equilibrium predictions [11]; furthermore, whenever in the liquid phase, more accurate, tabulated liquid-phase properties from the fuel database are employed.

Thermodynamic derivatives. Following the work by Trujillo et al. [8], all thermodynamic relationships in the FRESCO solver were updated to become EoS-neutral, including use for a variety of
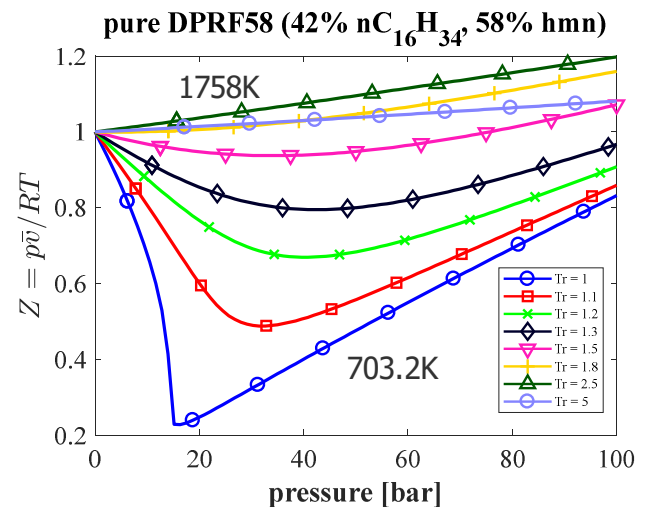

Figure 1. PR-EoS compressibility chart of a DPRF58 fuel mixture.

Peng-Robinson EoSes without any manipulation of the equations and linear system solvers. Furthermore, whenever any multiphase thermodynamic properties are needed (for example, by the chemistry or spray solvers), they are automatically gathered from the EoS being currently employed.

One relevant example is with the pressure solution equation within the SIMPLE procedure [23]: in each cell of the computational domain, it equates the thermodynamic volume following a change in state of the gas phase, with the Lagrangian volume following charge motion, according to the momentum equation:

$$V_{lag} = V_n + \Delta t \sum (\boldsymbol{u}_f \cdot \boldsymbol{A}_f); \qquad (4)$$

$$V_{ig} = V_p \left(1 - \frac{1}{\gamma}\left(\frac{p}{p_p} - 1\right)\right); \qquad (5)$$

p is the pressure field being sought; V_{lag} the Lagrangian volume and V_{ig} the thermodynamic ideal-gas approximation during some SIMPLE loop iteration; V_n the mesh volume before the Lagrangian step, $\boldsymbol{u}_f$ the face velocity field, $\boldsymbol{A}_f$ the face area vectors, γ the isentropic coefficient; and subscript p represents the solution at the end of the previous SIMPLE iteration. The relationship in Eq. 5 was extended to the actual Taylor series definition:

$$V_{EoS} = V_p + \left.\frac{\partial V}{\partial p}\right|_s \cdot (p - p_p) = V_p - \frac{M}{\rho^2 c_s^2}(p - p_p); \qquad (6)$$

where c_s is a now EoS-neutral isentropic speed of sound term.

Generalization of the thermodynamics properties and their derivatives yields results such as those reported in Figure 2: the ideal-gas EoS predictions act as high-pressure limit of the Peng-Robinson EoS. Besides conventional derivatives such as the specific heats c_p, c_v, the following were made available: dU/dT|$_p$ (int. energy derivative at constant pressure), c_s (sound speed [cm/s]), dp/dρ|$_{TY}$, γ, dV/dp|$_s$ and dV/dT|$_p$.

Phase Equilibrium solver

An improved version of the phase equilibrium solver by Qiu and Reitz [10] was implemented. This framework features testing of a single-phase, total compositional array which is fed to the multiphase space: if the whole mixture fed to the system is not stable as a single phase (i.e., its Gibbs free energy is not at global minimum), a two-phase mixture is assumed, and its phase split and composition of the two phases are computed. This procedure, also known as a TPn-*flash* calculation problem, is outlined in Figure 3:

1) First, several *(4+n_s)* trial equilibrium ratios are assumed for the single-phase stability tests: using a large number reduces the risk of finding local minima instead of the global minimum;

2) For each test, the single-phase stability analysis is run. This optimization problem features minimization of the modified tangent plane distance (TPD*) function, which employs the mixture's fugacity coefficients to evaluate equilibrium: a TPD>0 optimum corresponds to stable single-phase equilibrium. Since the TPD function is

strongly non-convex, a new hybrid solution scheme was implemented: a coarse tolerance solution is achieved with a limited number of successive substitution iterations (SSI); it is then used to initialize the usual BFGS method of [24].

3) To save CPU time, when at least 2 valid and useful optimized solutions are found from the initial set of trials, the solution with minimum optimum TPD is picked. If the optimal solution has TPD<0, then a single phase is not possible.

4) A two-phase split problem is run to find the relative phase molar fraction, λ, and its composition. The Rachford-Rice equations are solved with the method of Leibovici and Neoschil [25].

The constant-temperature flash calculation is also employed for more complex flash calculations such as for isobaric-isoenergetic (*HPn flash*) problems and adiabatic mixing of two phases. In these cases, the TPn solver is embedded in the nonlinear solution function, whose zero is sought for by employing Powell's hybrid solver [26]:

$$h_{multiphase}(T, \boldsymbol{z}_{feed}) = \lambda h_1 w_1 + (1 - \lambda) h_2 w_2, \qquad (7)$$
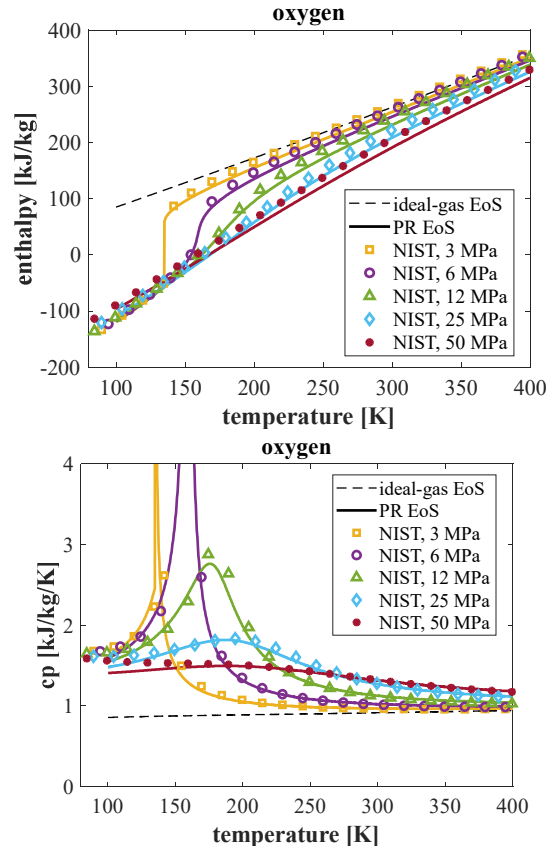
$$f(T) = (h_{target} - h_{multiphase})/h_{target}. \qquad (8)$$

Figure 2. Comparison of predicted oxygen specific enthalpy (top) and constant-pressure heat (bottom) data compiled from NIST webbook [27].
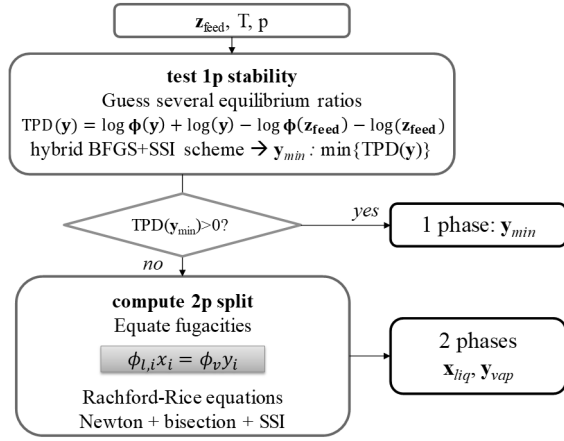
10/16/2019

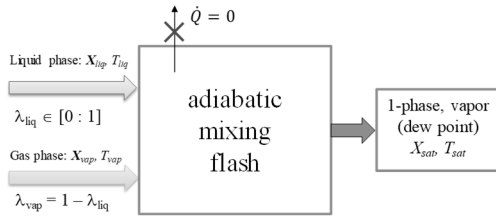Figure 3. Outline of the phase-equilibrium solver procedure.

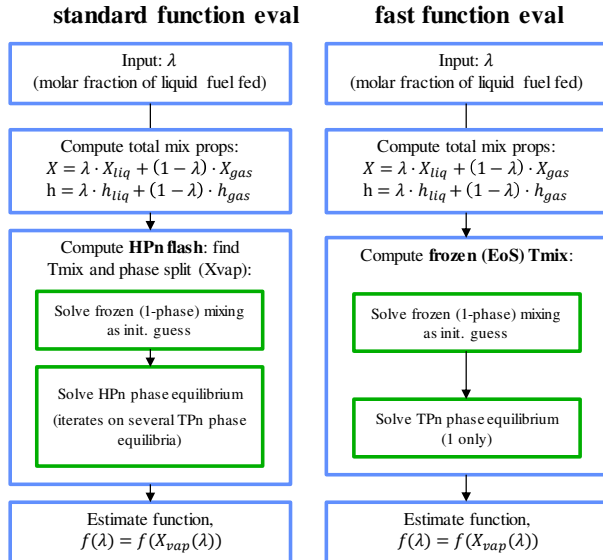Figure 4. Schematic representing the saturated mixing process.

Figure 5. Standard and fast work-flows for estimating the saturated mixing function.

Saturated mixing calculation. A different approach is employed whenever a saturated mixing calculation is requested. This calculation is critical to vaporization processes, where mixing between liquid fuel and gaseous air at a droplet's surface leads to a vapor phase at saturated (*dew point*) conditions. A schematic of this problem is presented in Figure 4: given the temperature and composition of two inlet phases, one must

10/16/2019

find the molar fraction of each of the two feed phases that leads, after an adiabatic mixing process, to a single phase in saturated vapor (*dew point*) conditions. Naming $\lambda_{liq} = x_{liq}$ the molar fraction of liquid feed phase, and $x_{vap} = 1 - \lambda_{liq}$ that of the gas feed phase, a continuous, differentiable function was defined:

$$f(x_{vap}) = \begin{cases} \left(\dfrac{x_{vap} - \bar{x}}{\bar{x}}\right)^2, & x_{vap} < \bar{x} \\ \left(\dfrac{x_{vap} - \bar{x}}{1 - \bar{x}}\right)^2, & x_{vap} \geq \bar{x} \end{cases} \tag{9}$$

which 1) is bound in $-1 \leq f \leq 1$ (good for convergence criteria), 2) it has a zero in $\bar{x} = 0.995$, i.e., numerically close enough to the dew point, but safely in the 2-phase region; 3) it is monotonic, i.e., it is suitable for safe bisection methods whenever the nonlinear solver fails. Figure 5 shows how the function of Equation 9 is computed: as there is only one phase at the dew point, one can assume that the total system temperature is the same both in the 1-phase and the 2-phase neighborhood (such as also shown later in Figure 7). By replacing the costly *HPn* flash calculation with one single *TPn* flash, more than 80% CPU time was saved for saturated mixing estimates on a 7-species multicomponent fluid.

Multi-phase behavior of diesel sprays

Whenever two separate phases exist, some Gibbs free energy of mixing is not being converted to the additional entropy of the mixed single phase; hence, system temperature will be higher. Figure 6 shows mixing temperatures of n-dodecane and nitrogen at Spray A-relevant conditions [6]: in the multiphase-region, a higher temperature is seen than the 'frozen' one being predicted by bare
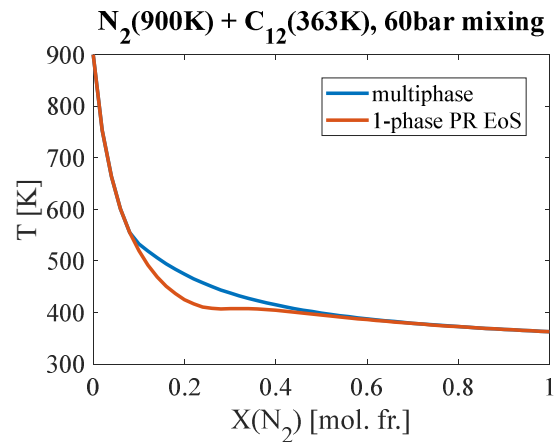

Figure 6. Comparison of single-phase and multiphase adiabatic mixing temperatures of liquid n-dodecane (T_{liq}=363K) and nitrogen (T_{vap}=900K) at 60 bar, showing temperature discrepancy up to $\Delta T_{mix} = 49.2K$ when not considering multiphase mixing.
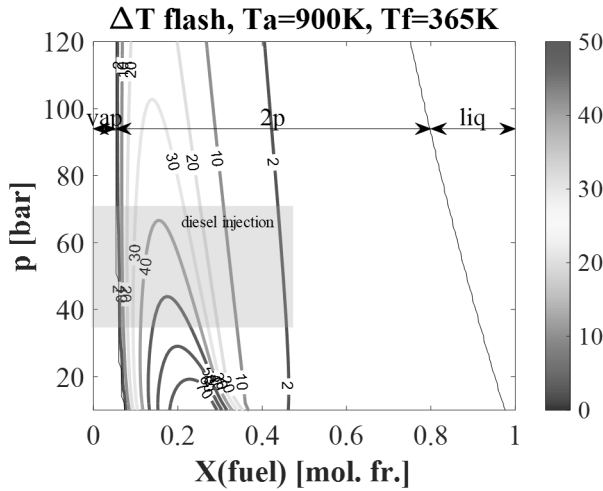
Figure 7. Temperature difference in a liquid DPRF58 (365K) in non-reactive gas (at 900K) mixing process at variable pressure. Shaded gray area: conditions relevant to fuel injection in diesel engines.

(single-phase) application of the PR EoS, with a peak $\Delta T_{mix} = 49.2K$ at a nitrogen fraction in the multiphase gas $X(N_2) = 0.2$. Following the diesel spray experiments of Siebers [28, 29], VLE analyses with a DPRF58 liquid fuel surrogate in a non-reacting charge (N_2:89.75, CO_2: 6.49; H_2O: 3.76) were conducted. In Figure 7, mixing temperatures highlight that significant temperature differences, up to ΔT_{flash}>70K overall, or approximately ΔT_{flash}~40K at diesel injection conditions can be observed whenever mixing diesel fuel and air with a multiphase solver, instead of with the single-phase PR EoS approach. These differences are expected to be relevant in the very rich core of the diesel spray jet, where the first ignitable mixture is formed.

Simulating multiphase mixing also affects the relative composition of the two-phase mixture, as the liquid phase contains some amount of dissolved gas, and vice versa.
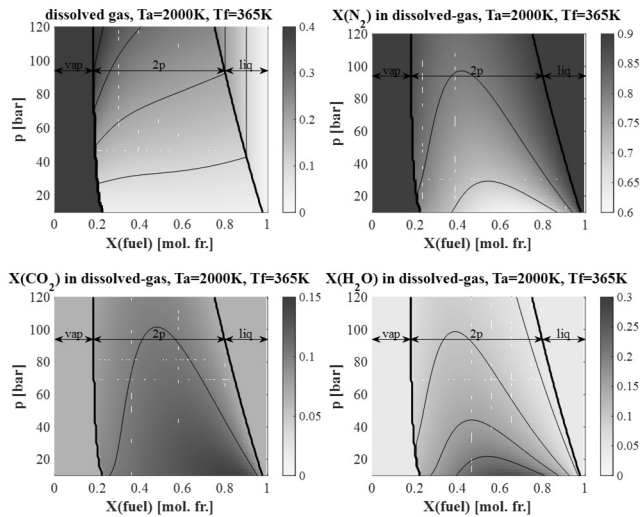

Figure 8. Dissolved gas behavior in multiphase diesel (365K) – combustion products (2000K) mixing. In clockwise order: mole fraction of gas components dissolved in the liquid phase; relative composition of the dissolved gas in the liquid phase: fraction of nitrogen, water, CO2.
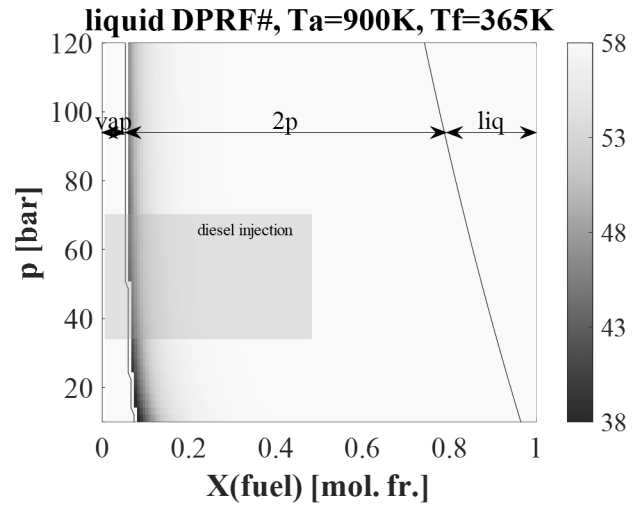

Figure 9. Diesel Primary Reference (DPRF) number of the liquid component after two-phase mixing of DPRF58 with combustion products.

Figure 8 summarizes predicted dissolved gas composition from adiabatic mixing of DPRF58 (365K) and combustion products (2000K), at conditions relevant to post-injections. A trend of increasing dissolved gas fraction in the liquid phase at increasing pressures is seen, with peak values exceeding 40% in volume at pressures greater than 100 bar. The dissolved gas composition is also sensitive to in-cylinder pressure: lower-pressure mixing leads to more CO_2- and water-rich liquid, while high-pressure mixing leads to more nitrogen being dissolved in the liquid fuel phase.

On the other hand, differential vaporization of the fuel components is seen, as summarized in Figure 9. Differences in composition of the vaporizing fuel lead to differences in its ignitability, as the composition:

$$DPRF = \frac{X(hmn)}{X(hmn)+X(nC_{16}H_{34})} \cdot 100, \qquad (10)$$

is directly related to its cetane number (CN=100 for DPRF0; CN=15 for DPRF100) [30]. When mixing DPRF58 with a 900K charge, the observed liquid-phase composition exhibited *lower* DPRF number (higher CN), signaling that the vaporized amount into the gas-phase charge had opposite behavior: higher gas-phase DPRF# and lower gas-phase CN, i.e., a less ignitable vapor mixture was found. This suggests that, to the extent that the composition of the liquid phase of the vaporizing spray is in equilibrium with the surrounding charge, the ignition delay of the vapor phase will be that of the original fuel if it can vaporize completely. But, if the mixture is so fuel-rich that two separate phases are found (for example, close to the spray jet's liquid core) the ignition delay of the vapor phase will be longer, because the less-ignitable HMN has lower critical conditions than n-hexadecane.

Liquid-Jet Phase-Equilibrium spray modeling

Limitations of state-of-the-art spray modeling approaches.
Lagrangian spray modeling features a sequence of separate phenomena, namely atomization, vaporization, collisions, drop dynamics. These models require several calibration constants,

and their mutual interaction is often non-trivial [15]. Moreover, the physics represented in these models often do not properly consider real-gas and multiphase thermodynamics.

Vaporization processes require knowledge of the saturated adiabatic mixing conditions. At the 'surface', or the interface between the drop's outer radius and the infinity gas phase, saturated vapor is a used as a boundary condition to compute an instantaneous surface regression rate [31]. Raoult's law of partial pressure is then used for
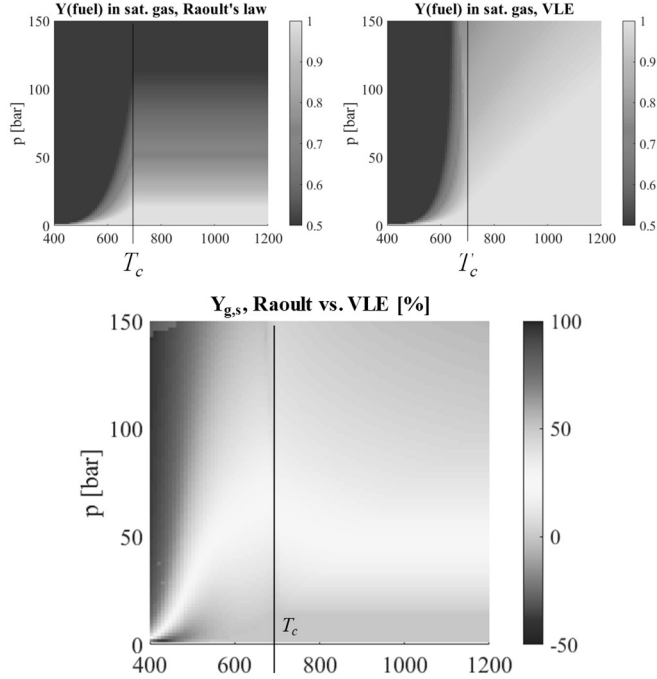
Figure 10. Predicted fuel components' mass fraction in saturated mixing of DPRF58 and combustion products according to (left) Raoult's law; (right) phase equilibrium solver. Bottom: percent discrepancy between the two approaches. X-axis represents the infinity gas-phase temperature.

both simplicity and speed; however, it is observed to yield significant error, as represented in Figure 10. For a DPRF58 + non-reacting charge mixture, the relative percent difference of the Raoult approximation versus the real-gas prediction varied between -41.1% and +99.94%; the contour plot showing greater deviations in the sub-critical gas-phase temperature range, but also in the high pressure range relevant to engine conditions; at the pseudo-critical temperature, the peak error was +46.3%.

Breakup models generally do not consider real-gas and multiphase effects as well. For the widely-adopted Kelvin-Helmholtz/Rayleigh-Taylor (KH-RT) model, a primary, slow drop size decay rate is computed based on linear perturbation theory of the liquid column [32]. After some characteristic breakup length L_{RT} is reached, catastrophic breakup into tiny droplets occurs, followed by complete vaporization quickly afterwards [15], as represented in Figure 11, where:

$$L_{RT} = 10.28998 \cdot C_{RT} d_n \frac{\sqrt{\pi}}{2} \sqrt{\frac{\rho_{liq}}{\rho_{gas}}}, \quad (11)$$

with $C_{RT} = 1.94$ or equated to the primary wavelength constant B_1:

$$10.28998 \cdot C_{RT} \frac{\sqrt{\pi}}{2} = B_1. \quad (12)$$

As shown in Figures 12 and 13, the KH-RT breakup length concept, that determines the overall liquid length, cannot capture real-gas effects. Whenever ambient density is held constant, the breakup length is constant too, and the pressure/temperature dependency observed in experiments cannot be matched with a single setup. When the temperature is changed, a unique density sweep line is seen instead of a band of liquid lengths.
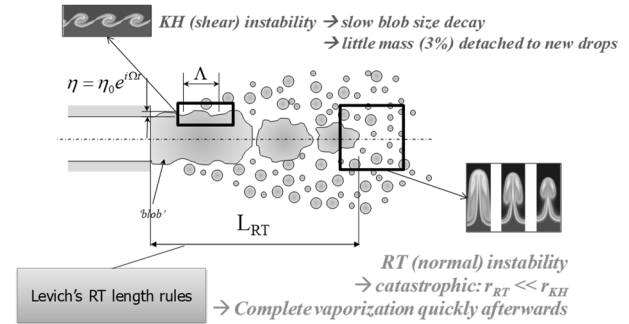

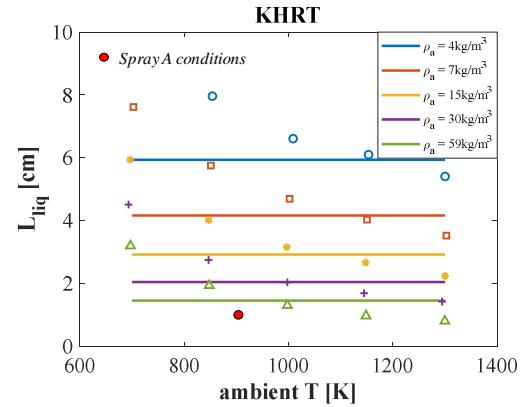Figure 11. Hybrid KH-RT breakup modeling approach schematic.

Figure 12. Comparison between KH-RT predicted primary breakup length (lines) and measured liquid length in the Sandia bomb [28] (markers) with liquid $nC_{16}H_{34}$ at varying ambient temperatures and densities.
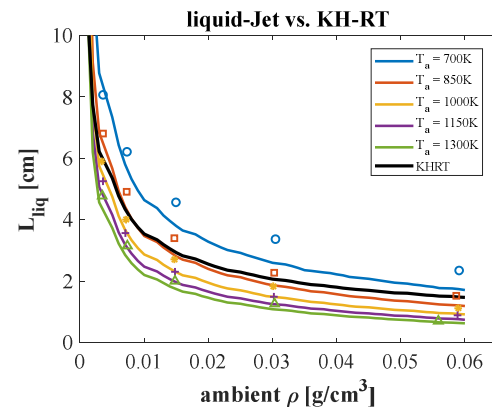

Figure 13. Comparison between KH-RT breakup length (black line), liquid-jet theory (colored lines) and measured liquid length (markers) in the Sandia bomb [28] with liquid hmn at varying ambient densities and temperatures.

Lagrangian Phase-Equilibrium spray model. The phase-equilibrium (EP) spray model by Yue and Reitz [12] based on Siebers's liquid-jet scaling [29] was implemented to assess its potential to overcome the limitations of traditional modeling approaches. This model assumes that the phase change process between the injector nozzle and the fully vaporized gas phase is mixing limited, and that local
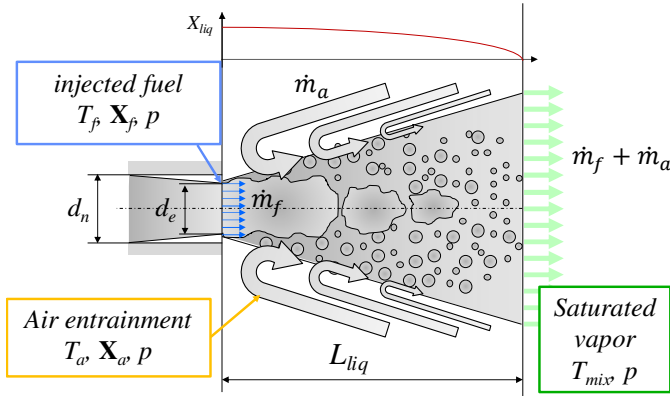

Figure 14. Schematic representing the liquid-jet phase-equilibrium spray model concept.

phase equilibrium conditions can be assumed, as represented in Figure 14.

The region surrounding the liquid jet represents a control volume where adiabatic mixing between the injected liquid fuel (with temperature T_f and composition X_f) and the entrained gaseous charge (T_a, X_a) takes place. The liquid length represents the end of the mixing region, i.e., where a single phase in saturated vapor conditions is found.

Based on mass conservation [29], the liquid-jet model predicts a liquid length:

$$L_{liq} = C_L x^+ \sqrt{\left(\frac{2}{B}+1\right)^2 - 1}, \qquad (13)$$

where C_L=0.41 is a calibration constant, $x^+ = c_D d_{noz}\sqrt{\rho_f/\rho_a}/(0.66\tan\theta/2)$ is the nozzle's length scaling parameter, and the phase equilibrium defines parameter B:

$$B = B(T_a, T_f, p, X_a, X_f) = \frac{\dot{m}_f}{\dot{m}_a}\bigg|_{sat} = \frac{\lambda_{sat}w(X_f)}{(1-\lambda_{sat})w(X_a)}, \qquad (14)$$

which represents the mass ratio between the liquid (fuel) and the gas (ambient) phase at the saturated mixing conditions found at the liquid length. Figure 15 represents contours of predicted B parameter for mixing relevant to engine vaporization processes. Saturated mixing of liquid n-dodecane at 400K with a gaseous air-fuel mixture made up of standard air with variable amounts of gas-phase dodecane is analyzed. The Spray A pressure of 60bar was used; gas-phase pressure and the amount of fuel in the inlet air-fuel vapor were varied. As Figure 15 shows with the dark blue region, at low enough temperatures, $B=0$, because any amount of liquid fuel mixed with the gas-phase will always lead to either a 2-phase or a single-phase liquid mixture: a saturated vapor mixture cannot be found here. At higher temperatures, there is one only B

value that leads to a saturated vapor, and some counter-intuitive behavior is seen. Let the reader consider an isotherm (a vertical line): i.e., neglecting the evaporative cooling associated with the formation of the air+fuel vapor mixture. The plot shows that per same temperature, an air-fuel gas mixture that has higher fuel content exhibits a higher value of B: i.e., when mixed, it needs a larger amount of liquid fuel feed before saturation is reached, even if the larger fuel molecules have higher critical point and exhibit stronger real-gas effects. However, they also increase the heat capacity of the gas-phase significantly; hence, when mixed with a low-temperature liquid, more of it is needed to reach saturation.
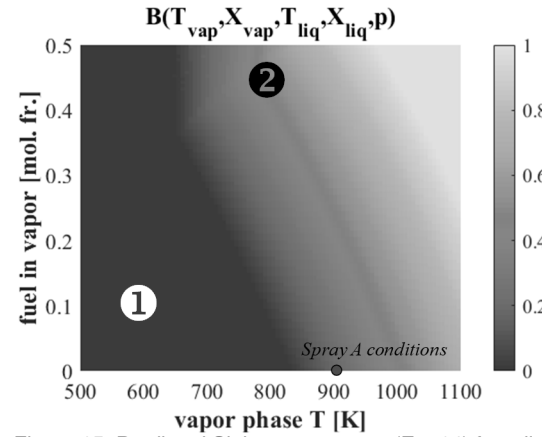

Figure 15. Predicted Siebers parameter (Eq. 14) for a liquid dodecane (T_f=400K) in air+dodecane vapor at 60 bar at variable temperature and mass fraction of fuel in the inlet vapor phase. Region 1: no saturated conditions possible for any amounts of fuel; region 2): vapor containing some fuel can accommodate more fuel than standard air.

Using this liquid length model, accurate predictions of the liquid length dependency on local pressure and temperature conditions are achieved, as reported in Figures 13 and 16. The calibration constant C_L employed by Siebers provides reasonable results out of the box. However, it should be noted that spray cone angle is another input to this model, which was observed to have a strong impact on the overall predicted length via x^+, and for which a predictive model is not yet available.
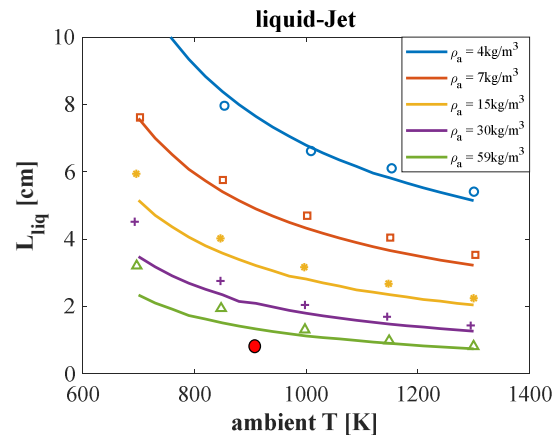

Figure 16. Comparison between liquid-jet length and measured liquid length in the Sandia bomb [28] with liquid $nC_{16}H_{34}$ at varying ambient temperatures. The red dot represents Spray A conditions.

10/16/2019

Lagrangian implementation and analysis

Following the modeling approach of Yue and Reitz [12], the liquid-jet phase-equilibrium model was implemented in the FRESCO CFD solver using Lagrangian parcels and a multiphase Eulerian solution. Different from standard modeling approaches, the Lagrangian parcel cloud is not meant to produce a meaningful spray representation; and, even though it retains geometrical location, it is mainly used as a momentum boundary condition for the Eulerian flow solver, serving the purpose of the liquid-jet model: that Eulerian modeling of the internal nozzle flow and dynamics is not necessary.

The Lagrangian parcels still release mass, energy and momentum to the Eulerian solver; however, instead of vaporizing to the gas phase, mass is transferred to the multiphase solution, which will then compute the phase status (1 or 2 phases) and relative composition using the phase equilibrium solver.

The EP model is implemented in a similar way as the gas-jet model [15], as represented in Figure 17. The Lagrangian parcels move freely according to the parcel momentum equations; their size – hence, the amount of mass being transferred to the Eulerian solver – is defined based on their location within the liquid jet. The liquid-jet is a conical region identified by the instantaneous liquid length, L_{liq}, and the spray cone angle θ. A liquid-jet size decay function is applied along the injection axis (x), while a Gaussian function is applied in the normal direction (z):

$$r(x, z, L_{liq}) = \frac{d_{32}}{2} \cdot \sqrt[3]{1 - \gamma(x, L_{liq})} \cdot G(z), \qquad (15)$$

d_{32} being the injected blob's diameter, γ the liquid-jet size decay function, and G the cross-flow gaussian size function.
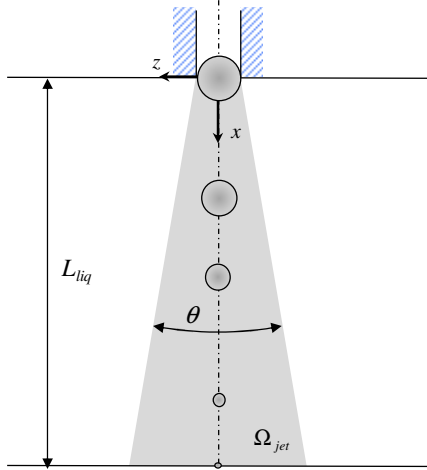

Figure 17. Schematic of the liquid-jet model application region and of prescribed Lagrangian-size behavior.

While the Gaussian size function is applied to ensure a smooth drop-size transition when parcels travel in crossflow and exit the liquid-jet region from the cone angle surface, the γ function of axial size decay controls the momentum transfer between the droplets and the Eulerian phase. Hence, the γ function was chosen such that the Lagrangian parcel mass follows a liquid-

jet/gas-jet analogy, with drop mass decay similar to the gas-jet momentum/velocity decay function of [33]:

$$\gamma = \frac{\sqrt{1 + 16(x/x^+)^2} - 1}{\sqrt{1 + 16(L_{liq}/x^+)^2} - 1}; \qquad (16)$$

The origin of momentum decay along the injection axis is also shifted by an amount equal to the gas-jet velocity decay location:

$$x_0 = \frac{3 d_{jet}}{K_{entr}} = \frac{3 d_{noz}}{K_{entr}} \sqrt{\frac{\rho_f}{\rho_a}}, \qquad (17)$$

where the gas-jet entrainment constant, K_{entr}, controls the start-of-velocity-decay location and can be seen as a control knob for momentum transfer to the Eulerian phase.
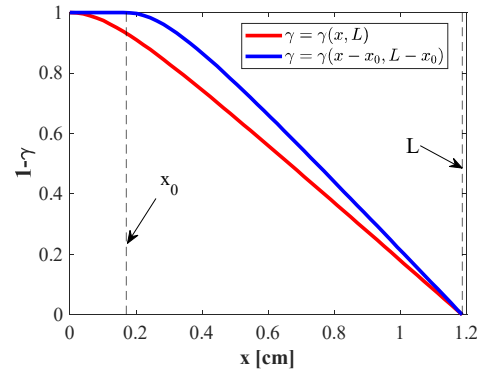

Figure 18. Lagrangian size decay function via gas-jet velocity decay location [15].

Spray A. The Engine Combustion Network Spray A experiment [34] was used to assess performance of the FRESCO implementation of the liquid-jet/phase equilibrium model. The Spray A simulation setup of [14] was used with the GRNG k-epsilon turbulence model and a full-360 degree mesh with a 1mm resolution at the nozzle, similar to that used in engineering-level diesel engine simulations. As Figure 20 shows, excellent agreement with the well-validated KH-RT setup of [15] could be achieved with limited calibration: the liquid length constant, controlling liquid penetration, was increased to CL=0.75, and the gas-jet entrainment constant was reduced to K_{entr} = 0.5. Note that the need for a different entrainment scaling with the EP model was needed for correct momentum transfer because the Lagrangian size distribution achieved by the γ function is different than the radial distribution effects the KH-RT model has. A representation of this phenomenon is given in Figure 19: with the EP model, Lagrangian parcels whose mass and momentum have not yet been released to the Eulerian phase, fill the whole spray cone angle. Future investigations will look at ways to represent reasonable breakup-like radial size distributions. Also, no Eulerian liquid phase fuel was observed in the computational mesh at any times: this is consistent with the observations of Matheis and Hickel [6], which showed that for Spray A, liquid fuel density is only observed in a tiny thin region close to the injection centerline, requiring a micron-sized mesh to observe.

Predicted fuel fraction distribution along the spray jet as compared with the experimental images is reported in Figure 21. The comparison shows that consistent liquid/vapor penetration predictions
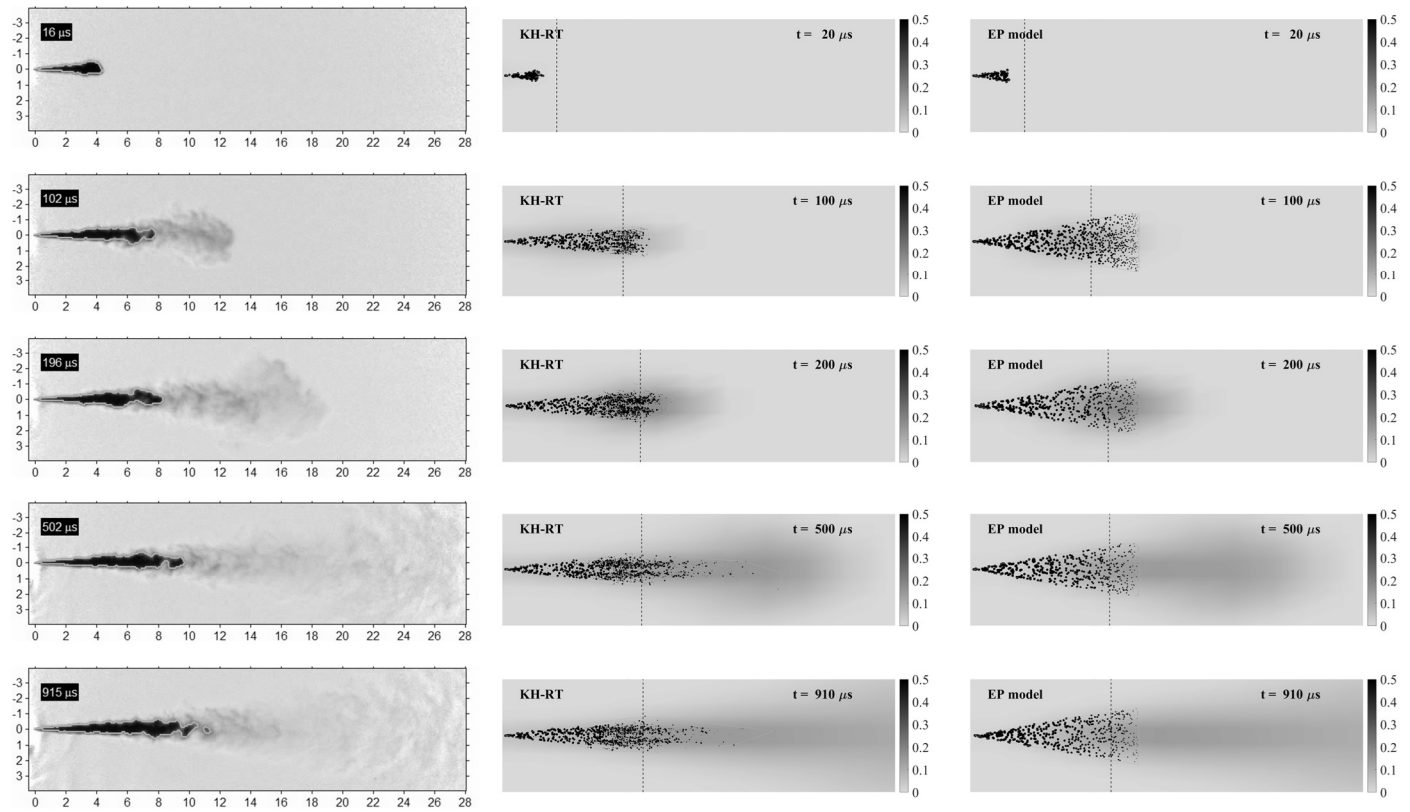
Figure 19. Comparison between imaged and simulated Spray A liquid and vapor jet structure (Manin et al. [4]). (left) experimental image; (center) KH-RT model; (right) EP model.

also lead to consistent mixture distribution predictions with the two spray models. For the EP model, a slightly more disperse jet is seen; and an accurate representation of the spray jet structure was achieved.

Concluding remarks

In this work, we implemented the Peng-Robinson Equation of State and a phase equilibrium solver and coupled them with the FRESCO CFD code. These tools were employed to analyze the effects of real-gas and multiphase behavior on state-of-the-art spray modeling approaches, and to test a new Equilibrium-Phase ('EP') spray model. This approach employs Lagrangian parcels only as carriers to distribute mass and momentum to the Eulerian CFD solver, where a multiphase solution is computed. Regarding multiphase mixing as well as liquid length and Spray A experiments, the following conclusions could be drawn:

- Multiphase modeling via real-gas EoS and VLE calculations captures the complex behavior of multicomponent fuels, including differential vaporization of fuel components at different compositional and thermodynamic conditions;

- The accuracy of a single-phase real-gas EoS is limited compared with a true multiphase solution, because of its inability to capture the conversion of Gibbs free energy of mixing to entropy, which leads to local temperature differences of several tens of degrees Kelvin;

- Standard spray modeling approaches fail at capturing real-gas effects significantly: breakup models only depend on ambient density, and not on p-T behavior; vaporization models apply
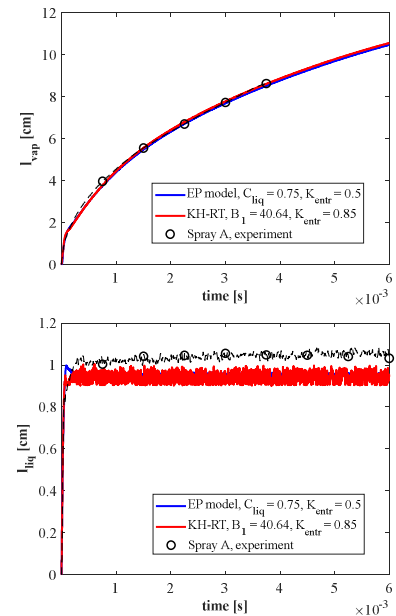

Figure 20. Comparison between predicted and experimental Spray A vapor penetration (top) and liquid penetration (bottom).
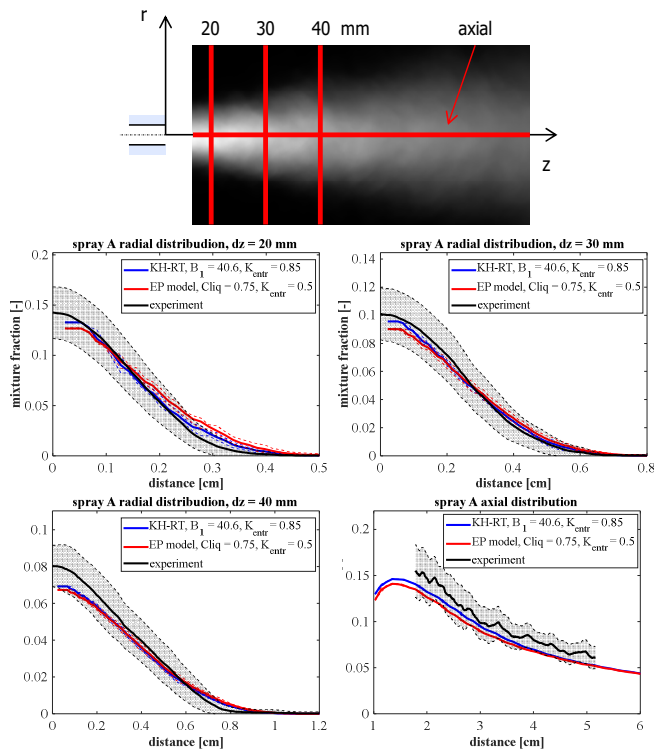
10/16/2019

Figure 21. Comparison between predicted and experimental Spray A fuel vapor distributions. Shaded areas bounded by dashed lines represent ± one standard deviation of the azimuthal average.

simplified saturated mixing BCs whose error compared to real gas models can be greater than 100%;

- Employing Phase Equilibrium with the Liquid-Jet theory (EP model) to model sprays is a promising alternative to standard spray modeling approaches: it produces accurate results with a significantly simpler framework; its only calibration parameters are the liquid-length constant and the entrainment constant.

Future work will be devoted to continuing validation of the EP model framework against experiments with non-reacting and reacting conditions, as well as real-world diesel engine simulations; and to testing multiphase behavior with different fuels.

References

[1] R. N. Dahms, J. Manin, L. M. Pickett and J. C. Oefelein, "Understanding high-pressure gas-liquid interface phenomena in Diesel engines," *Proceedings of the Combustion Institute,* vol. 34, no. 1, pp. 1667-1675, 2013.

[2] C. Crua, J. Manin and L. M. Pickett, "On the transcritical mixing of fuels at diesel engine conditions," *Fuel,* vol. 208, no. 1, pp. 535-548, 2017.

[3] N. Neal and D. Rothamer, "Measurement and characterization of fully transient diesel fuel jet processes in an optical engine with production injectors," *Experiments in Fluids,* vol. 57, p. 155, 2016.

[4] J. Manin, M. Bardi, L. M. Pickett, R. N. Dahms and J. C. Oefelein, "Microscopic investigation of the atomization and mixing processes of diesel sprays injected into high pressure and temperature environments," *Fuel,* vol. 134, no. 1, pp. 531-543, 2014.

[5] R. Dahms and J. C. Oefelein, "Liquid jet breakup regimes at supercritical pressures," *Combustion and Flame,* vol. 162, no. 10, pp. 3648-3657, 2015.

[6] J. Matheis and S. Hickel, "Multi-component vapor-liquid equilibrium model for LES of high-pressure fuel injection and application to ECN Spray A," *International Journal of Multiphase Flow,* vol. 99, no. 1, pp. 294-311, 2018.

[7] C. Rodriguez, P. Koukouvinis and M. Gavaises, "Simulation of supercritical diesel jets using the PC-SAFT EoS," *The Journal of Supercritical Fluids,* vol. 145, no. 1, pp. 48-65, 2019.

[8] M. F. Trujillo, P. J. O'Rourke and D. Torres, "Generalizing the Thermodynamics State Relationships in KIVA-3V," Los Alamos National Laboratories LA-13981, Los Alamos, NM, 2002.

[9] M. F. Trujillo, D. J. Torres and P. J. O'Rourke, "High-pressure multicomponent liquid sprays: Departure from ideal behaviour," *International Journal of Engine Research,* vol. 5, no. 3, pp. 229-246, 2004.

[10] L. Qiu and R. D. Reitz, "Development of a thermodynamically consistent, robust and efficient phase equilibrium solver and its validations," *Fuel,* vol. 115, no. 1, pp. 1-16, 2014.

[11] L. Qiu and R. D. Reitz, "An investigation of thermodynamic states during high-pressure fuel injection using equilibrium thermodynamics," *International Journal of Multiphase Flow,* vol. 72, no. 1, pp. 24-38, 2015.

[12] Z. Yue and R. D. Reitz, "An equilibrium phase spray model for high-pressure fuel injection and engine combustion simulations," *International Journal of Engine Research,* vol. 20, no. 2, pp. 203-215, 2019.

[13] F. Perini and R. D. Reitz, "FRESCO - an object-oriented, parallel platform for internal combustion engine simulations," in *28th International Multidimensional Engine Modeling User's Group Meeting at the SAE Congress*, Detroit, 2018.

[14] F. Perini, S. Busch, K. Zha and R. D. Reitz, "Comparison of Linear, Non-linear and Generalized RNG-based k-epsilon models for turbulent diesel engine flows," in *SAE Technical Paper 2017-01-0561*, Detroit, MI, 2017.

[15] F. Perini and R. D. Reitz, "Improved atomization, collision and sub-grid scale momentum coupling models for transient vaporizing engine sprays," *International Journal of Multiphase Flows,* vol. 79, pp. 107-123, 2016.

[16] F. Perini, E. Galligani and R. D. Reitz, "A study of direct and Krylov iterative solver techniques to approach linear scaling of the integration of Chemical Kinetics with detailed combustion mechanims," *Combustion and Flame,* vol. 161, no. 5, pp. 1180-1195, 2014.

[17] F. Perini, S. Busch, K. Zha, R. D. Reitz and E. Kurtz, "Piston Bowl Geometry Effects on Combustion Development in a High-Speed Light-Duty Diesel Engine," in *SAE Technical Paper 2019-24-0167*, Capri, Italy, 2019.

[18] F. Perini, K. Zha, S. Busch, E. Kurtz, R. C. Peterson, A. Warey and R. D. Reitz, "Piston geometry effects in a light-duty, swirl-supported diesel engine: flow structure characterization," *International Journal of Engine Research,* vol. OnlineFirst, 2017.

[19] F. Perini, S. Busch, E. Kurtz, A. Warey, R. C. Peterson and R. D. Reitz, "Limitations of Sector Mesh Geometry and Initial Conditions to Model Flow and Mixture Formation in Direct-Injection Diesel Engines," in *SAE Techical Paper 2019-01-0204*, Detroit, 2019.

[20] D.-Y. Peng and D. B. Robinson, "A New Two-Constant Equation of State," *Ind. Eng. Chem. Fundamen.,* vol. 15, no. 1, pp. 59-64, 1976.

[21] O. Hasan and S. I. Sandler, Modeling Vapor-Liquid Equilibria, Cambridge University Press, 1998.

[22] M. L. Michelsen and J. M. Mollerup, Thermodynamic models: fundamentals & computational aspects, Holte, Denmark: Tie-Line Publications, 2004.

[23] D. J. Torres and M. F. Trujillo, "KIVA-4: An unstructured ALE code for compressible gas flow with sprays," *Journal of Computational Physics,* vol. 219, no. 2, pp. 943-975, 2006.

[24] H. Hoteit and A. Firoozabadi, "Simple Phase Stability-Testing Algorithm in the Reduction Method," *AIChE Journal,* vol. 52, no. 8, pp. 2909-2920, 2006.

[25] C. F. Leibovici and J. Neoschil, "A solution of Rachford-Rice equations for multiphase systems," *Fluid Phase Equilibria,* vol. 112, no. 1, pp. 217-221, 1995.

[26] M. J. Powell, "A Hybrid Method for Nonlinear Equations," in *Numerical Methods for Nonlinear Algebraic Equations XI*, London, Ph. Rabinowitz, 1970.

[27] "NIST Chemistry Webbook," National Institute of Standards and Technology, 1 10 2018. [Online]. Available: https://webbook.nist.gov/chemistry/. [Accessed 01 10 2019].

[28] D. L. Siebers, "Liquid-Phase Fuel Penetration in Diesel Sprays," *SAE Transactions Journal of Engines,* vol. 107, no. 3, pp. 1205-1227, 1998.

[29] D. L. Siebers, "Scaling Liquid-Phase Fuel Penetration in Diesel Sprays Based on Mixing-Limited Vaporization," *SAE Transactions Journal of Engines,* vol. 108, no. 3, pp. 703-728, 1999.

[30] American Society for Testing and Materials, "D-613 Standard Test Method for Cetane Number of Diesel Fuel Oil," ASTM, West Conshohocken, PA, 2017.

[31] D. J. Torres, P. J. O'Rourke and M. F. Trujillo, "A Discrete Multicomponent Fuel Model," *Atomization and Sprays,* vol. 13, no. 2&3, p. 42, 2003.

[32] J. C. Beale and R. D. Reitz, "Modeling Spray Atomization with the Kelvin-Helmholtz/Reyleigh-Taylor Hybrid Model," *Atomization and Sprays,* vol. 19, no. 7, pp. 623-650, 1999.

[33] N. Abani and R. R. Reitz, "Unsteady turbulent round jets and vortex motion," *Physics of Fluids,* vol. 19, no. 1, p. 125102, 2007.

[34] "ECN Data Search Page," [Online]. Available: https://ecn.sandia.gov/ecn-data-search/. [Accessed 28 08 2018].

[35] S.-K. Kim, H.-S. Choi and Y. Kim, "Thermodynamic modeling based on a generalized cubic equation of state

10/16/2019

for kerosene/LOx rocket combustion," *Combustion and Flame,* vol. 159, no. 1, pp. 1351-1365, 2012.

[36] A. Bader, P. Keller, C. Hasse and B. Meyer, "The influence of non-ideal vapor-liquid-equilibrium on vaporization of multicomponent hydrocarbon fuels," in *ICLASS 2012, 12th Triennal International Conference on Liquid Atomization and Spray Systems*, Heidelberg, 2012.

Contact Information

Federico Perini
Federico.Perini@w-erc.com

Acknowledgments

10/16/2019